

Spatial-dispersion-induced acoustic anisotropy in semiconductor structures

F. Alsina,* P. V. Santos, and R. Hey

Paul-Drude-Institut für Festkörperelektronik, Hausvogteiplatz 5–7, D-10117 Berlin, Germany

(Received 21 November 2001; published 19 April 2002)

We demonstrate that a Rayleigh surface acoustic wave (SAW) propagating on the surface of a (001)-oriented GaAs quantum well structure induces different optical properties for propagation directions along the $[110]$ and the $[\bar{1}10]$ symmetry axes. The nonequivalence of the two directions is attributed to the lift of the fourfold rotation symmetry of the optical and acoustic properties around the $[001]$ growth axis by the finite wave vector of the SAW, a spatial dispersion effect which is also expected for bulk modes in zinc blende semiconductors.

DOI: 10.1103/PhysRevB.65.193301

PACS number(s): 77.65.Dq, 77.65.Ly, 78.20.Hp, 78.55.–m

The symmetry properties of elementary excitations in a crystal are mainly determined by the crystal point group. In addition, nonlocal effects make these properties also dependent on the wave vector \mathbf{q} of the excitation, a phenomenon called spatial dispersion.¹ For excitations with wavelengths much larger than the lattice constant, such as elastic waves and photons in the visible range, spatial dispersion is normally small; as a result, the $\mathbf{q}=0$ limit applies and their symmetry becomes imposed by the crystal point group. Under appropriate conditions, however, a nonvanishing \mathbf{q} may lower the symmetry relative to the crystal. Interesting examples of the reduction in symmetry of the optical properties of cubic semiconductors include the intrinsic optical anisotropy² and the pressure-induced optical activity,³ which are of second and first order in q , respectively.

Spatial dispersion also affects the symmetry of vibrational modes.⁴ These effects are particularly interesting in polar crystals, where vibrations with a nonvanishing \mathbf{q} may induce a macroscopic electric polarization field. The electron-phonon interaction becomes mediated not only by the ordinary deformation potential but also by the piezoelectric (for acoustic phonons) or Fröhlich (for optical phonons) mechanisms associated with the polarization field. Recently, Ilisavskii *et al.*⁵ reported differences in acoustoelectric properties induced by a reversal in propagation direction of elastic modes in $\text{La}_{0.67}\text{Ca}_{0.33}\text{MnO}_3$ layers on LiNbO_3 , which were attributed to an interference between the deformation and piezoelectric mechanisms. In zinc blende semiconductors, the interference between the deformation potential and the Fröhlich interactions induced by a LO mode propagating along the $z=[001]$ direction leads to different Raman polarizabilities along the $x'=[110]$ and $y'=[\bar{1}10]$ axes.⁶ In this Brief Report, we show that the superposition of the two mechanisms induced by an acoustic mode in (Al,Ga)As quantum well (QW) structures also removes the invariance of the optical properties under a 90° rotation around the $z=[001]$ growth axis. Specifically, we demonstrate that the phase relationship between the acoustic (\mathbf{u}) and the piezoelectric (Φ) fields composing the wave function of elastic modes differs by 180° for modes propagating along the x' and y' axes, thus leading to different optical properties. The phase difference, which is also expected in zinc blende crystals, arises from the distinct transformation properties of the two fields under a 90° rotation of the crystal.

The investigations were performed by using photoluminescence (PL) spectroscopy to map the acoustic and the piezoelectric fields induced by a surface acoustic wave of the Rayleigh type (SAW) propagating on the QW structure. The samples consist of a 12-nm GaAs QW with $\text{Al}_{0.3}\text{Ga}_{0.7}\text{As}$ barriers grown by molecular-beam epitaxy on GaAs (001). The QW is placed 100 nm below the surface. SAW's propagating along the x' and the y' surface directions were generated by identical aluminum split-finger interdigital transducers (IDT's) deposited on the sample surface, as illustrated in the inset of Fig. 1. The IDT's were designed for operation at a wavelength λ_{SAW} of $5.6 \mu\text{m}$, corresponding to a frequency $\omega_{\text{SAW}}/(2\pi)$ of 520 MHz at 12 K. The PL measurements were carried out at 12 K using a confocal microscope with illumination and detection areas with a diameter of about $2 \mu\text{m}$. The continuous radiation from a Ti:sapphire laser ($\lambda_L=765 \text{ nm}$) was employed as excitation source. The setup also allows for interferometric measurements of the vertical (i.e., parallel to z) surface displacement induced by the SAW, which was used to determine the absolute magnitude of the SAW acoustic field. The latter will be specified in terms of the ratio P_l between the acoustic power and the width of the SAW beam.

Photoluminescence spectra of the GaAs QW recorded under SAW's propagating along the two perpendicular directions x' and y' are shown in Figs. 1(a) and 1(b), respectively, for different values of P_l . In the absence of a SAW, the PL spectrum displays a main emission line at 1.5388 eV corresponding to the electron-heavy hole (e -hh) excitonic transition. The much weaker line at 1.5462 meV is associated with the electron-light hole (e -lh) transition, which becomes visible due to the high excitation intensities (approximately 100 W/cm^2) produced by the focused illumination. In addition to these two well-defined emission lines, a third structure appears as a shoulder on the low energy side of the e -hh line (indicated by an asterisk in the figures). The dependence of the PL on excitation intensity and on temperature indicates that this structure arises from excitons localized on potential fluctuations in the QW plane.

Under the influence of a SAW, the PL intensity becomes strongly suppressed (note the logarithmic vertical scale in Fig. 1) as a consequence of (i) the ionization of the photoexcited excitons^{7–9} and of (ii) the sweep of the electron-hole pairs out of the microscopic PL detection spot by the longi-

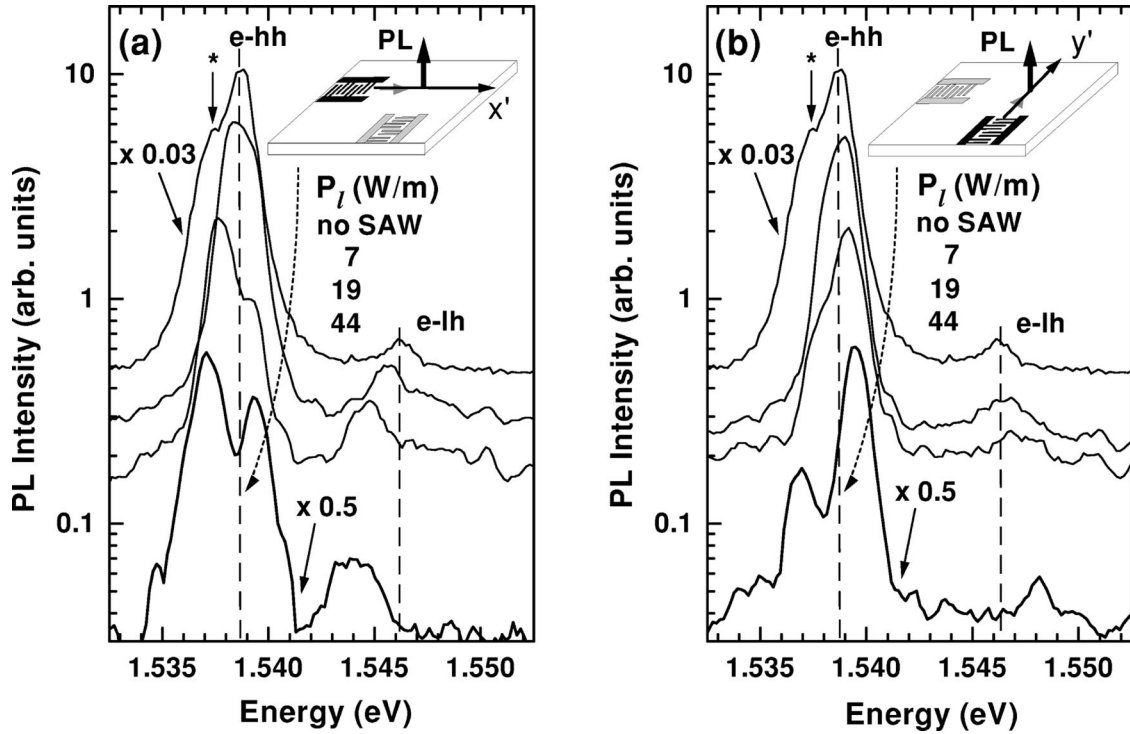


FIG. 1. PL spectra of a 12-nm GaAs/Al_{0.3}Ga_{0.7}As single QW in the absence and under the influence of a surface acoustic wave with power density P_l propagating along the (a) $x' = [110]$ and (b) $y' = [\bar{1}10]$ directions.

tudinal component of the piezoelectric field, which moves with the SAW propagation velocity v_{SAW} .^{9,10} The structure associated with localized excitons disappears already for very low P_l levels, thus indicating that the carriers become delocalized. In addition, PL lines split into two components with energies $E_{e\text{-hh}}^{+(-)} = E_{e\text{-hh}}^0 + \Delta E_{e\text{-hh}}^{+(-)}$ ($E_{e\text{-lh}}^{+(-)} = E_{e\text{-lh}}^0 + \Delta E_{e\text{-lh}}^{+(-)}$ for the $e\text{-lh}$ transitions) with increasing SAW amplitude. The splitting is attributed to the sinusoidal band-gap modulation induced by the SAW strain field, which leads to two transitions with a high joint density of states with an energy separation $\Delta E_{e\text{-hh(lh)}} = \Delta E_{e\text{-hh(lh)}}^+ - \Delta E_{e\text{-hh(lh)}}^-$.¹⁰

The degree of PL quenching in Fig. 1 is approximately the same for SAW's propagating along the x' and y' directions. The relative intensities of the low and high energy components of the PL doublets, however, differ considerably for the two propagation directions. In fact, while for SAW's launched along y' the oscillator strength of the $e\text{-hh}$ and $e\text{-lh}$ lines concentrates on the high energy doublet component, SAW propagation along x' leads to the enhancement of the low energy component.¹¹ Due to the larger strain splitting, the transfer of oscillator strengths becomes particularly pronounced for the $e\text{-lh}$ transitions, where the high (low) energy component practically disappears in Fig. 1(a) [Fig. 1(b)] for high P_l levels. These results clearly demonstrate that different optical properties are obtained for SAW propagation along the x' and y' symmetry axes.

In order to understand the difference in oscillator strength for the two propagation directions, we first recall that while the type-I potential modulation by the SAW strain field determines the recombination energies, the relative intensities of the different components of the PL line are dictated by the

much stronger type-II modulation induced by the piezoelectric field, which controls the spatial distribution of the electron (n) and hole (p) densities.¹² The latter also depends on the transport properties of the carriers, which determine their ability to follow the dynamic potential. The highly mobile electrons can readily follow the dynamic modulation; they remain, therefore, concentrated close to the maxima of the piezoelectric potential. In contrast, the lower mobility of the holes leads to a wider spatial distribution of the hole density p in the SAW potential. As a consequence, the recombination probability (proportional to the product np) peaks at the same position as the electron concentration n . The difference in oscillator strengths for the PL doublets in Figs. 1(a) and 1(b) indicates distinct charge distribution for SAW's propagating along the x' and y' axes, and, thus, different phase relationships between the acoustic and piezoelectric fields.

The phase relationship between \mathbf{u} and Φ becomes clear if we consider that the longitudinal (u_j) and transverse (u_z) displacement fields of a Rayleigh SAW propagating along the $\mathbf{j}(\mathbf{j}\parallel x'$ or $\mathbf{j}\parallel y')$ direction of the (001) surface can be written as^{13,14}

$$u_j(j, z, t) = u_{j,0}(z) e^{i\phi} \quad (1)$$

and

$$u_z(j, z, t) = i u_{z,0}(z) e^{i\phi}, \quad (2)$$

respectively, where $u_{j,0}(z)$ and $u_{z,0}(z)$ are real functions, and $\phi = k_{\text{SAW}}j - \omega_{\text{SAW}}t$, with $k_{\text{SAW}} = 2\pi/\lambda_{\text{SAW}}$, denotes the SAW phase. The previous equations hold for weak piezoelectric materials, as is the case of GaAs. Equations (1) and (2) yield

three nonvanishing strain components u_{jj} , u_{zz} , and u_{jz} , which induce a dynamic volume change $s_0 = (u_{jj} + u_{zz})$. The strain also induces an electric polarization field $\mathbf{P}(j,t) = \pm ie_{14}[u_{jj}(j,z_0,t)\mathbf{z} + 2u_{jz}(j,z_0,t)\mathbf{j}]$, where e_{14} denotes the piezoelectric constant and the positive and negative signs apply for $\mathbf{j} \parallel x'$ and $\mathbf{j} \parallel y'$, respectively. From Eqs. (1) and (2), the hydrostatic contribution to the band-gap modulation¹⁵ $E_g^{\text{hyd}} = a_h s_0$ and the piezoelectric potential Φ induced in the QW plane $z = z_0$ can be expressed as

$$\Delta E_g^{\text{hyd}}(j,t) = ia_h k_{\text{SAW}} [u_{j,0}(z_0) + u'_{z,0}(z_0)] e^{i\phi}, \quad (3)$$

$$\Phi(j,t) = \pm ie_{14} \left[u_{z,0}(z_0) - \frac{u'_{j,0}(z_0)}{k_{\text{SAW}}} \right] e^{i\phi}, \quad (4)$$

respectively, where the prime denotes derivation with respect to z and a_h is the hydrostatic deformation potential. Several important conclusions can be drawn from the previous expressions.

The change in sign in the expressions for Φ and $\mathbf{P}(j,t)$ is associated with the transformation properties of the third rank piezoelectric tensor, which require that $e_{ijk} = -e_{jik}$. Since all quantities within the square brackets in Eqs. (3) and (4) are real and the band-gap modulation is mainly determined by ΔE_g^{hyd} , the relative phase between the piezoelectric potential and the band-gap modulation changes by 180° when the SAW propagation direction varies from x' to y' , in agreement with the results in Fig. 1.

With regard to the piezoelectric properties, the SAW can be viewed as a combination of a longitudinal and a shear bulk wave with strain fields u_{jj} and u_{jz} , respectively. Each of these waves generate an electric polarization field perpendicular to its propagation direction, which change sign under a 90° rotation of the crystal. Therefore, the results obtained for a SAW in the QW structures also apply for longitudinal and transverse bulk elastic waves propagating along a $\langle 110 \rangle$ direction in zinc blende semiconductors.

The reversal in sign is due to the different orientations of the chains of Ga and As atoms along the $[110]$ and $[\bar{1}10]$ directions, which leads to distinct polarization fields under an elastic mode, as illustrated for a pure shear wave in Fig. 2. Note that the electromagnetic restoring force is the same for the two configurations, so that the energy degeneracy of the modes is not lifted.

The symmetry reduction investigated in this work is of first order in the elastic properties, and, in contrast to the acoustic activity,⁴ does not rely on higher order components of the elastic tensor.

In order to obtain quantitative data for the band-gap modulation and for the potential distribution, we calculated numerically the acoustic and piezoelectric fields induced by the SAW in the QW plane. From the strain field, the modulation of the conduction and valence bands was then determined following the method described in Ref. 10. The absolute amplitude of the SAW fields was determined by measuring the SAW vertical displacement field ($u_{z,0}$) using interferometry. The modulation of the hydrostatic strain component s_0 and of the energy $\Delta E_{e\text{-hh}}$ ($\Delta E_{e\text{-lh}}$) of the $e\text{-hh}$ ($e\text{-lh}$) transition calculated for a SAW with $u_{z,0} = 0.3$ nm

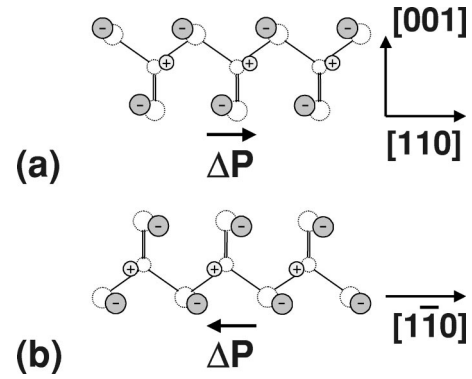


FIG. 2. Microscopic atomic positions in equilibrium (open circles), and under a pure shear wave u_{jz} propagating along the (a) $\mathbf{j} = [110]$ and (b) $\mathbf{j} = [\bar{1}10]$ directions (dashed circles). The small and large circles denote Ga and As atoms, respectively, and ΔP is the polarization field.

(corresponding to $P_l = 18.5$ W/m) are displayed in Fig. 3(a) and 3(b), respectively. The modulation amplitudes $\Delta E_{e\text{-hh}}$ and $\Delta E_{e\text{-lh}}$ differ from the hydrostatic value ΔE_g^{hyd} in Eq. (3) due to the strain-induced coupling between the hh and lh bands. The latter leads to a significantly larger splitting for the $e\text{-lh}$ transition, in agreement with Fig. 1.

The potential distribution in the QW plane is illustrated in Fig. 3(c) for SAW's propagating along the x' (solid squares) and y' directions (circles). The potential modulation, which is over two orders of magnitude larger than the band-gap modulation, tends to accumulate electrons at the positions of

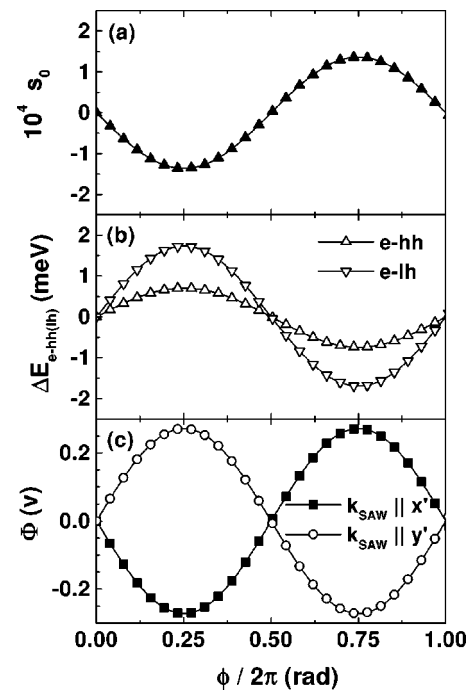


FIG. 3. (a) Hydrostatic strain $s_0 = u_{jj} + u_{zz}$, (b) strain-induced modulation of the electron-heavy hole ($\Delta E_{e\text{-hh}}$) and electron-light hole ($\Delta E_{e\text{-lh}}$) transitions, and (c) piezoelectric potential Φ induced by a SAW with a power density of $P_l = 18.5$ W/m as a function of the SAW phase $\phi = k_{\text{SAW}} j - \omega_{\text{SAW}} t$.

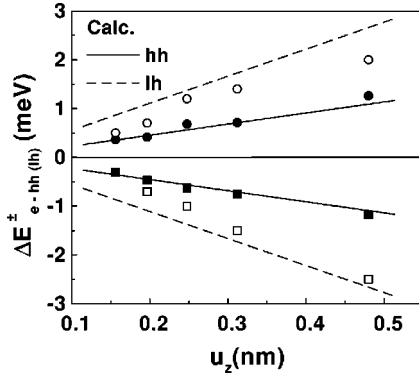


FIG. 4. Strain induced splittings of the e -hh (filled symbols) and e -lh (open symbols) as a function of the amplitude u_z of the transverse field of a SAW propagating along x' (circles) and y' (squares). The solid and dashed lines display the calculated energy modulation of the two transitions.

maximum and minimum gap for $k_{\text{SAW}}||y'$ and $k_{\text{SAW}}||x'$, respectively. The different charge distributions lead to the distinct oscillator strengths in the PL spectra of Fig. 1.

A further comparison between the experiments and calculations is illustrated in Fig. 4. The solid and hollow circles in

this figure show the energy shifts ΔE_{e-hh}^+ and ΔE_{e-lh}^+ of the higher intensity doublet component for $k_{\text{SAW}}||y'$, measured for different SAW amplitudes. The squares represent the corresponding data (i.e., ΔE_{e-hh}^- and ΔE_{e-lh}^-) determined for SAW propagation along x' . The SAW intensity is stated in terms of the measured vertical displacement amplitude $u_{z,0}(z=0)$. The lines, which were calculated using the model described above, show a good agreement with the measured energy shifts.

In conclusion, we have used PL spectroscopy to demonstrate that a SAW propagating on the (001) surface of a zinc blende semiconductor induces different optical properties for propagation directions along the $[110]$ and $[\bar{1}10]$ symmetry axes. The nonequivalent properties arise from different phase relationships between the acoustic and piezoelectric components of the SAW field for the two propagation directions. The latter is attributed to the distinct transformation properties of the acoustic and piezoelectric components of the SAW field under a 90° rotation of the crystal.

We thank M. Giehler for comments and for a critical reading of the manuscript. Support from the Deutsche Forschungsgemeinschaft (Project No. SA598/2-1) is gratefully acknowledged.

*Email address: falsina@pdi-berlin.de

¹V. M. Agranovitch and V. L. Ginzburg, *Crystal Optics with Spatial Dispersion and Excitons* (Springer, Heidelberg, 1984).

²P. Y. Yu and M. Cardona, *Solid State Commun.* **9**, 1421 (1971).

³P. Etchegoin and M. Cardona, *Solid State Commun.* **82**, 655 (1992).

⁴D. L. Portigal and E. Burstein, *Phys. Rev.* **170**, 673 (1968).

⁵Y. Ilisavskii *et al.*, *Phys. Rev. Lett.* **87**, 146 602 (2001).

⁶J. Menéndez and M. Cardona, *Phys. Rev. Lett.* **51**, 1297 (1983).

⁷K. S. Zhuravlev *et al.*, *Appl. Phys. Lett.* **70**, 3389 (1997).

⁸C. Rocke *et al.*, *Phys. Rev. Lett.* **78**, 4099 (1997).

⁹P. V. Santos, M. Ramsteiner, and F. Jungnickel, *Appl. Phys. Lett.* **72**, 2099 (1998).

¹⁰T. Sogawa *et al.*, *Phys. Rev. B* **63**, R121 307 (2001).

¹¹In previous publications (Refs. 10 and 12) the splitting and transfer of oscillation intensities have only been measured for a SAW's propagating along the $[\bar{1}10]$ direction.

¹²F. Alsina *et al.*, *Phys. Rev. B* **64**, R041 304 (2001).

¹³R. Stoneley, *Proc. R. Soc. London, Ser. A* **232**, 447 (1955).

¹⁴S. Simon, *Phys. Rev. B* **54**, 13 878 (1996).

¹⁵P. Yu and M. Cardona, *Fundamentals of Semiconductors: Physics and Materials Properties* (Springer, Heidelberg, 1995).